Title

Effects of topographic smoothing on the simulation of winter precipitation in High Mountain Asia

Journal

Journal of Geophysical Research: Atmospheres, 122(3)

ISSN

2169-897X

Authors

Cannon, Forest
Carvalho, Leila MV
Jones, Charles
et al.

Publication Date

2017-02-16

DOI

10.1002/2016jd026038

Peer reviewed

AGU PUBLICATIONS

JGR

Journal of Geophysical Research: Atmospheres

RESEARCH ARTICLE
10.1002/2016JD026038

Key Points:
- Smooth topography allows for the intensification of atmospheric circulation and generates stronger cross-barrier winds
- Precipitation distributions in smoothed topography experiments are biased relative to simulation with more realistic topography
- Smoothed topography simulation biases extreme events toward enhanced dynamics and thermodynamics

Correspondence to:
F. Cannon,
fcannon@geog.ucsb.edu

Citation:
Cannon, F., L. M. V. Carvalho, C. Jones, J. Norris, B. Bookhagen, and G. N. Kiladis (2017), Effects of topographic smoothing on the simulation of winter precipitation in High Mountain Asia, *J. Geophys. Res. Atmos.*, *122*, 1456–1474, doi:10.1002/2016JD026038.

Received 30 SEP 2016
Accepted 14 JAN 2017
Accepted article online 19 JAN 2017
Published online 2 FEB 2017

Effects of topographic smoothing on the simulation of winter precipitation in High Mountain Asia

Forest Cannon[1,2], Leila M. V. Carvalho[1,2], Charles Jones[1,2], Jesse Norris[1,2], Bodo Bookhagen[3], and George N. Kiladis[4]

[1]Department of Geography, University of California, Santa Barbara, California, USA, [2]Earth Research Institute, University of California, Santa Barbara, California, USA, [3]Institute of Earth and Environmental Science, University of Potsdam, Potsdam, Germany, [4]Physical Sciences Division, NOAA Earth System Research Laboratory, Boulder, Colorado, USA

Abstract Numerous studies have projected future changes in High Mountain Asia water resources based on temperature and precipitation from global circulation models (GCMs) under future climate scenarios. Although the potential benefit of such studies is immense, coarse grid-scale GCMs are unable to resolve High Mountain Asia's complex topography and thus have a biased representation of regional weather and climate. This study investigates biases in the simulation of physical mechanisms that generate snowfall and contribute to snowpack in High Mountain Asia in coarse topography experiments using the Weather Research and Forecasting model. Regional snowpack is event driven, thus 33 extreme winter orographic precipitation events are simulated at fine atmospheric resolution with 6.67 km resolution topography and smoothed 1.85° × 1.25° GCM topography. As with many modified topography experiments performed in other regions, the distribution of precipitation is highly dependent on first-order orographic effects, which dominate regional meteorology. However, we demonstrate that topographic smoothing enhances circulation in simulated extratropical cyclones, with significant impacts on orographic precipitation. Despite precipitation reductions of 28% over the highest ranges, due to reduced ascent on windward slopes, total precipitation over the study domain increased by an average of 9% in smoothed topography experiments on account of intensified extratropical cyclone dynamics and cross-barrier moisture flux. These findings identify an important source of bias in coarse-resolution simulated precipitation in High Mountain Asia, with important implications for the application of GCMs toward projecting future hydroclimate in the region.

1. Introduction

Developing future water management and planning strategies require the estimation of current and future precipitation magnitudes and variability [*Wehner*, 2013]. In recent years, a large number of studies have employed global circulation models (GCM) to estimate future precipitation in High Mountain Asia [e.g., *Lutz et al*., 2013; *Kapnick et al*., 2014; *Palazzi et al*., 2013, 2014; *Shea et al*., 2015]. The work of *Palazzi et al.* [2014] analyzed the properties of precipitation in western High Mountain Asia as simulated by 32 state-of-the-art GCMs participating in the Coupled Model Intercomparison Project phase 5 (CMIP5) [*World Climate Research Program,* 2011). They found that the multimodel ensemble mean and most individual models exhibit a wet bias with respect to observations in western High Mountain Asia for all seasons and the models differ considerably in their representation of seasonal climatologies. In general, no single model (or group of models) consistently outperformed all others for all the statistics considered, and the large spread in the behavior of individual models warrants caution in evaluating multimodel ensemble means over high topography [*Palazzi et al*., 2014]. Despite model uncertainty, a number of studies have utilized ensemble mean precipitation and temperature from GCMs to drive hydrologic models under future climate conditions and project changes in High Mountain Asia's water resources [e.g., *Lutz et al*., 2013; *Shea et al*., 2015; *Soncini et al*., 2015; *Su et al*., 2016]. *Miller et al.* [2012] provides a synthesis of previous studies projecting hydroclimate changes in High Mountain Asia. Though uncertainty in GCM-simulated precipitation is not well understood, a pertinent concern for High Mountain Asia is the effect of topographic resolution on the simulation of orographic forcing in the region's complex topography.

CMIP5 GCMs typically have horizontal grid resolutions of between 1 and 3°. Consequently, they have coarse topography and unrealistically represent regional topographic forcing of weather and climate [*Yorgun and Rood*, 2015]. The current study investigates how topographic smoothing affects the simulation of the primary drivers of precipitation in western High Mountain Asia. Extratropical cyclones are the primary climatic

influence in High Mountain Asia during nonmonsoon months [*Singh et al*., 1995; *Lang and Barros*, 2004; *Barlow et al*., 2005; *Dimri et al*., 2015], delivering in excess of 50% of the total annual precipitation in the western regions [*Lang and Barros*, 2004; *Barlow et al*., 2005; *Barros et al*., 2006; *Bookhagen and Burbank*, 2010; *Cannon et al*., 2014; *Wulf et al*., 2016]. These winter events, termed "westerly disturbances" (WD), generate heavy orographic precipitation when moisture flux along the cyclone's front encounters High Mountain Asia's topography. The majority of WD-generated precipitation falls as snow over the Karakoram and western Himalaya's high mountains, thus augmenting the region's snowpack and glaciers [*Anders et al*., 2006; *Tahir et al*., 2011; *Ridley et al*., 2013; *Cannon et al*., 2015].

Among extreme winter precipitation events, there is considerable variability in the dynamic and thermodynamic influences on precipitation. Available moisture, atmospheric stability and strength, and orientation of cross-barrier winds that drive orographic uplift all vary on an event-by-event basis [*Cannon et al*., 2015, 2016]. This manuscript details the effects of topographic smoothing on simulated relationships between cross-barrier winds, moisture availability, and orographic precipitation in High Mountain Asia and quantifies bias in the representation of precipitation in coarse topography simulation. In reference to previous studies that have identified significant influences of topographic resolution over meteorological simulation [e.g., *Mass et al*., 2002; *Colle*, 2008; *Gutmann et al*., 2012], modified topography experiments performed over High Mountain Asia in the present study are unique in their focus on real WD events and their control of horizontal resolution. The Weather Research and Forecasting (WRF) model is used to simulate 33 WD events during winter using both 6.67 km resolution topography and smoothed $1.85° \times 1.25°$ GCM topography. Differences in the generation of orographic precipitation are quantified across experiment types by evaluating the absolute magnitude and percentage change of dynamic and thermodynamic mechanisms. Identifying bias improves understanding of uncertainty in GCM representation of regional climate and is essential for the prudent application of GCM output toward projecting water resources availability in High Mountain Asia, as well as other mountainous regions.

2. Data

2.1. In Situ Data

Data from seven in situ stations located at low elevations of the Karakoram aid in the selection of extreme precipitation events for the WRF simulations. A reference map of the study region and station locations is shown in Figure 1. Here we consider daily accumulated precipitation from 7 Pakistani Meteorological Department (PMD) stations for the period 1979–2012. We assume that extant biases in the magnitude of station-measured precipitation in the Karakoram and western Himalaya [*Hewitt*, 2014] are constant in time and thus do not affect the selection of extreme events relative to all other dates in the record [*Cannon et al*., 2016].

2.2. Meteorological Data From Reanalyses

Climate Forecast System Reanalysis (CFSR) data, from the National Centers for Environmental Prediction [*Saha et al*., 2010], are used to investigate the large-scale climate and dynamics of WD, as well as to initialize WRF simulations. CFSR is available at 0.5° horizontal resolution for the period 1979–2013. CFSR was chosen on account of its spatial resolution and modern data assimilation system [*Saha et al*., 2010].

2.3. Extreme Precipitation Event Definition

Analyses of individual events are performed based on the identification of extreme precipitation using a combination of CFSR and PMD station data [*Cannon et al*., 2016]. First, principal component analysis of the data from PMD stations for November–April was performed using a covariance matrix to reduce the number of variables by identifying a leading orthogonal pattern of precipitation variability across all seven stations from 1979 to 2012 [*Wilks*, 2006]. The first principal component explained 53% of the variability among stations and high values were observed to correspond to high-magnitude precipitation at multiple PMD stations. CFSR, which was not included in the PCA analysis, also exhibited heavy precipitation over the western Himalaya and Karkoram during peaks in the first principal component. Independent 90th percentile dates (only the highest-magnitude day of all consecutive 90th percentile days is retained) from the station-based first principal component time series and independent 90th percentile dates from aggregated CFSR precipitation in the western Himalaya and Karakoram (73–77°E, 34–37°N) produced a collection of extreme

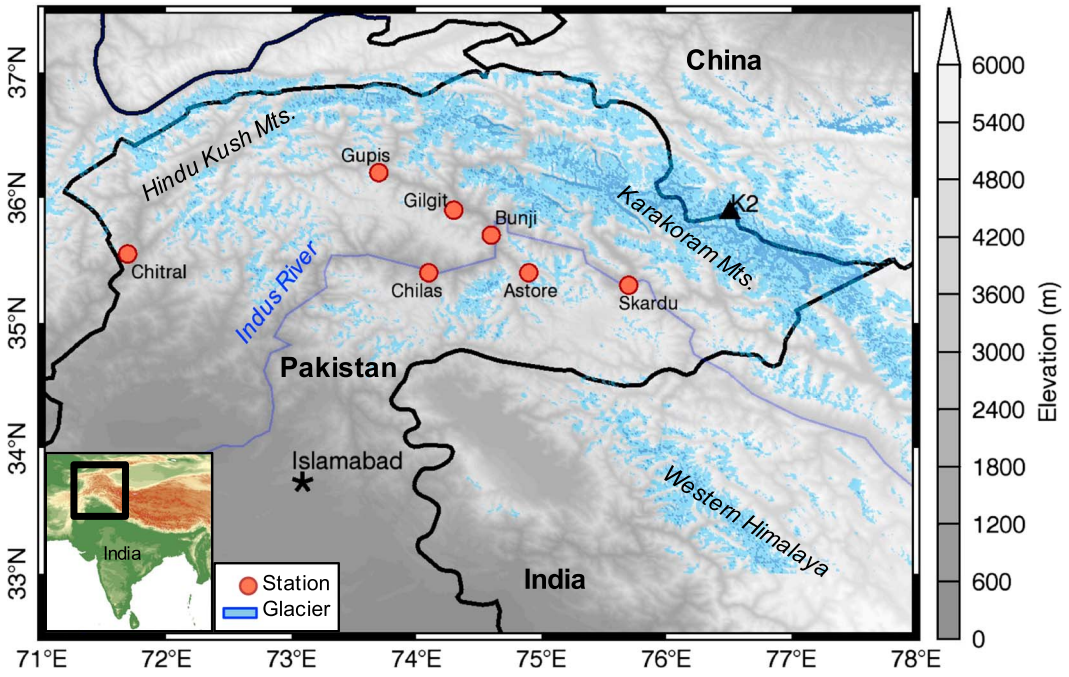

Figure 1. Topography map of the study area and station data locations (red circles). International borders are outlined in black. Blue shading indicates glacier coverage. The inset map shows the location of the study region (black box) over color-shaded topography.

precipitation events that overlapped in 205 cases, or approximately 67% of the time (PMD had 295 independent events and CFSR had 308), during November–April 1979–2012. For this work we dynamically downscale only 33 of the 205 extreme events on account of limited computing resources. Details on the event selection process are given in section 4.

3. Model Configuration

Each 1 day extreme precipitation event was simulated using version 3.7 of the Advanced Research Weather and Forecasting (ARW-WRF; hereafter WRF) model [*Skamarock et al.*, 2008]. For each selected date, 36 h simulations were initialized at 12 UTC the day preceding the event, with the first 12 h of simulation being discarded as "spin-up" [*Maussion et al.*, 2014]. Simulations were performed with two domains using one-way interaction, with an outer domain horizontal resolution of 20 km and an inner domain resolution of 6.67 km (3:1 ratio) on a Mercator projection (similar to *Norris et al.*, 2015, 2016). An adaptive time step with an upper limit of 120 s for the outer domain and 45 s for the inner domain was used. Initial and lateral boundary conditions were garnered from CFSR.

The parameterization schemes employed are as follows and were justified in *Norris et al.* [2015]: Thompson microphysics [*Thompson et al.*, 2008], Yonsei University boundary layer [*Hong et al.*, 2006], Fifth-Generation Mesoscale Model (MM5) Monin-Obukhov surface layer [*Monin and Obukhov*, 1954], Noah land surface [*Niu et al.*, 2011], Rapid Radiative Transfer Model (RRTM) longwave radiation [*Mlawer et al.*, 1997], Dudhia shortwave radiation [*Dudhia*, 1989], and Kain-Fritsch convection [*Kain*, 2004], outer domain only. Although convection is not parameterized in the inner domain, the 6.67 km resolution that is used does not adequately resolve deep convection or orographic convection, which is typically shallower and smaller in horizontal scale. *Norris et al.* [2015] performed thorough testing of this particular configuration. They concluded that although no single configuration is ideal across all conditions, this particular setup demonstrated the most realistic results for WD simulations in High Mountain Asia. WRF uses a terrain following vertical coordinate (50 levels in these simulations), but output has been interpolated to pressure levels for this discussion.

We additionally performed simulations of the 33 extreme events using coarse resolution topography to test how regional meteorology and orographic precipitation are modified when simulated over GCM-type

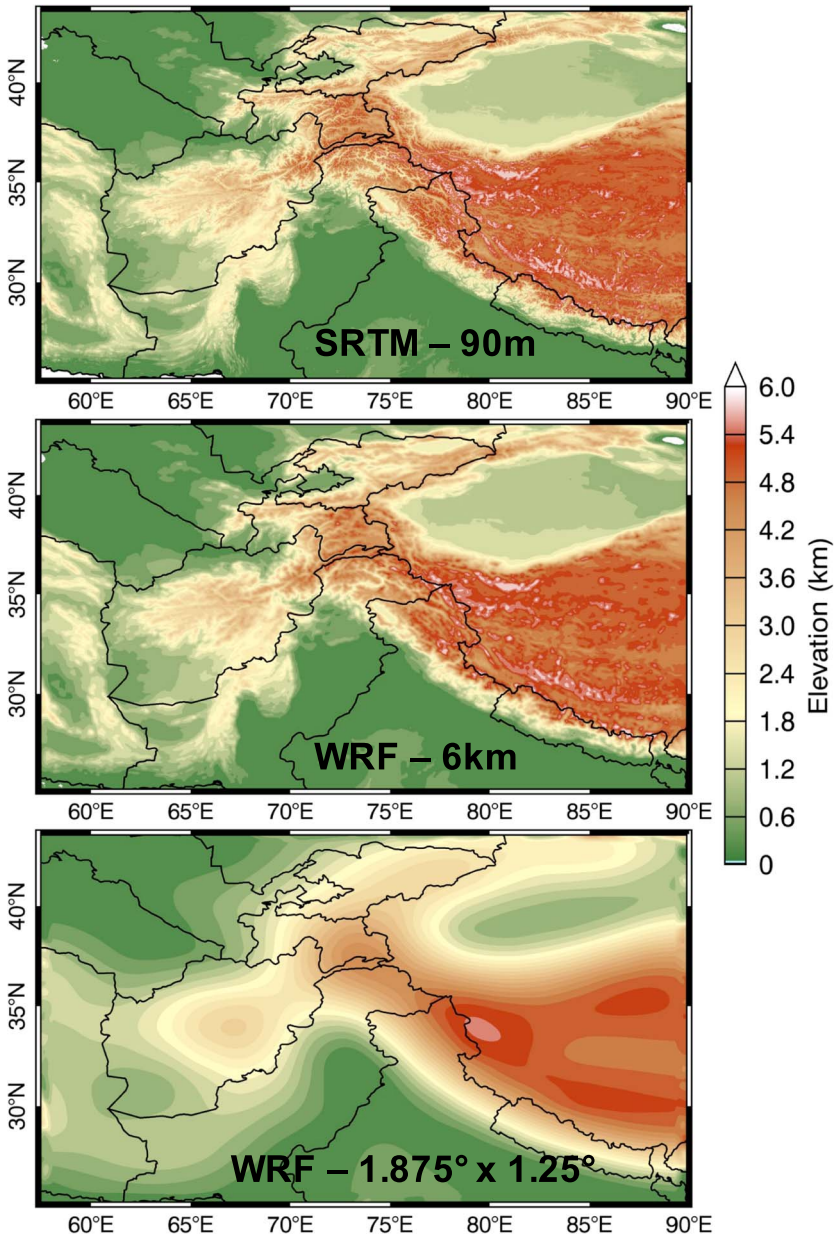

Figure 2. Shuttle radar topographic mission 90 m resolution topography (top), WRF original topography (6.67 × 6.67 km; middle), and WRF smoothed topography (~175 × 140 km; bottom). International borders are outlined in black.

topography. Modified topography experiments were performed using topography from the Hadley Center global circulation model (HadGEM2-ES) [*Martin et al.*, 2011) (1.875° × 1.25° horizontal resolution) that was resized to 6.67 km resolution, smoothed using cubic convolution interpolation to remove steep transitions across grid cells [*Park and Schowengerdt*, 1983], and then resampled onto WRF's grid. The mean elevations of the two topography experiments' domains are within 10 m. A 90 m digital elevation model from the Shuttle Radar Topography Mission [*Farr et al.*, 2007], the original 6.67 km topography, and modified topography for the High Mountain Asia study region are shown in Figure 2. The spatial extent of the topography figures corresponds to the spatial extent of WRF's inner domain for this study. The WRF configuration for original and modified topography experiments is identical except for changes to the input topography characteristics (elevation and slope) in the geographic information (geogrid) file. Static input to the WRF preprocessing system that may be affected by topography, such as land use categories, were not altered because the 36 h simulation of winter events was found to be insensitive to

these in previous testing (not shown). Simulations of 48 h (24 h spin-up) and 72 h (48 h spin-up) were tested for several events without significant differences from the 36 h simulations with 12 h of spin-up presented here. The computation time required for each simulation restricted sensitivity tests of different topographic smoothing techniques and horizontal resolutions. However, while the smoothing technique applied may alter the magnitude of the statistics presented, the processes that underlie the key findings of this research are robust. This research emphasizes the physical effect of smooth topography on the simulation of precipitation mechanisms rather than focusing on statistical differences alone. It is important to note that the modified topography experiments resolve small-scale precipitation processes that are not resolved at GCM-scales; thus, precipitation in a GCM likely differs from the high-resolution experiments with GCM topography.

Previous studies have identified the importance of model resolution in simulating the spatial distribution of precipitation [e.g., *Mass et al*., 2002; *Gao et al*., 2006; *Gutmann et al*., 2012]. This study is unique in its focus on topographic effects, which is made possible by maintaining consistent resolution (6.67 km) for both experiment groups. Controlling for horizontal resolution, which may generate model sensitivity as an artifact of possibly erroneous or inconsistent assumptions in the parameterizations schemes at different resolutions [*Giorgi and Marinucci*, 1996], allows for a more direct investigation of the role of topographic forcing on the simulated events.

4. Extreme Event Categories

Cannon et al. [2015] found extreme winter precipitation events in western High Mountain Asia to be driven by two primary mechanisms: (1) dynamical forcing, related primarily to the strength of cross-barrier winds that force moisture against topography, and (2) thermodynamic forcing, related to moisture availability and instability, which enhances orographic precipitation in the cross-barrier flow.

Here events are categorized based upon the findings of *Cannon et al.* [2016], which indicated that intraseasonal variability associated with the Madden Julian Oscillation (MJO) [*Madden and Julian*, 1972] significantly influences dynamic and thermodynamic drivers of precipitation during WD events in High Mountain Asia [*Barlow et al*., 2005; *Hoell et al*., 2014; *Cannon et al*., 2016]. Using the MJO index of *Jones* [2009]; *Cannon et al.* [2016] explained that phases of the MJO propagation cycle that favor the dynamical enhancement of WD through an extratropical Rossby wave response (phases 3 and 4; when enhanced convection is positioned over the eastern Indian Ocean and Maritime Continent) simultaneously suppress available moisture over southwest Asia [*Cannon et al*., 2016]. In these phases strong orographic forcing compensates for relatively little available moisture to produce extreme precipitation during WD events. As the MJO propagates the primary driver of precipitation in WD transitions so that in phases 7 and 8 (suppressed convection over the eastern Indian Ocean and Maritime Continent) WD exhibits relatively weak dynamics, while precipitation generation is attributable to large quantities of moisture exported from the tropics. In addition, the 205 extreme precipitation events identified in section 2.3 were categorized by MJO influence during neutral periods of the El Nino–Southern Oscillation (ENSO). Simulations were performed for 33 events from the following three MJO categories, representing differing contributions of dynamical and thermodynamic forcing to orographic precipitation: (1) The 13 events that occurred during MJO phases 7 and 8 with ENSO neutral, (2) the 10 events that occurred during MJO phases 3 and 4 with ENSO neutral, and (3) the 10 largest-magnitude precipitation events during neutral MJO and ENSO.

Figure 3 shows average significant (t test; $p < 0.05$) precipitable water and 500 hPa geopotential height anomalies (annual cycle removed) from CFSR for extreme events that occurred in MJO phases 7 and 8 (top), phases 3 and 4 (middle), and neutral phases [*Jones*, 2009]. The neutral condition group exhibits a well-developed trough, with minimum geopotential height of −90 gpm, west of High Mountain Asia. Cyclonic winds along the leading edge of the system draw upon a considerable moisture supply extending from the tropics around the Horn of Africa. These precipitation events are driven by strong contributions from both dynamical forcing and available moisture. In comparison, events in MJO phases 3/4 exhibit slightly deeper geopotential height anomalies (minimum of −105 gpm), leading to stronger cross-barrier winds and orographic forcing, while enhanced available moisture is observed only over the Gangetic Plain. Events in MJO phases 7/8 exhibit a relatively shallow trough (~−30 gpm), but a significant moisture plume

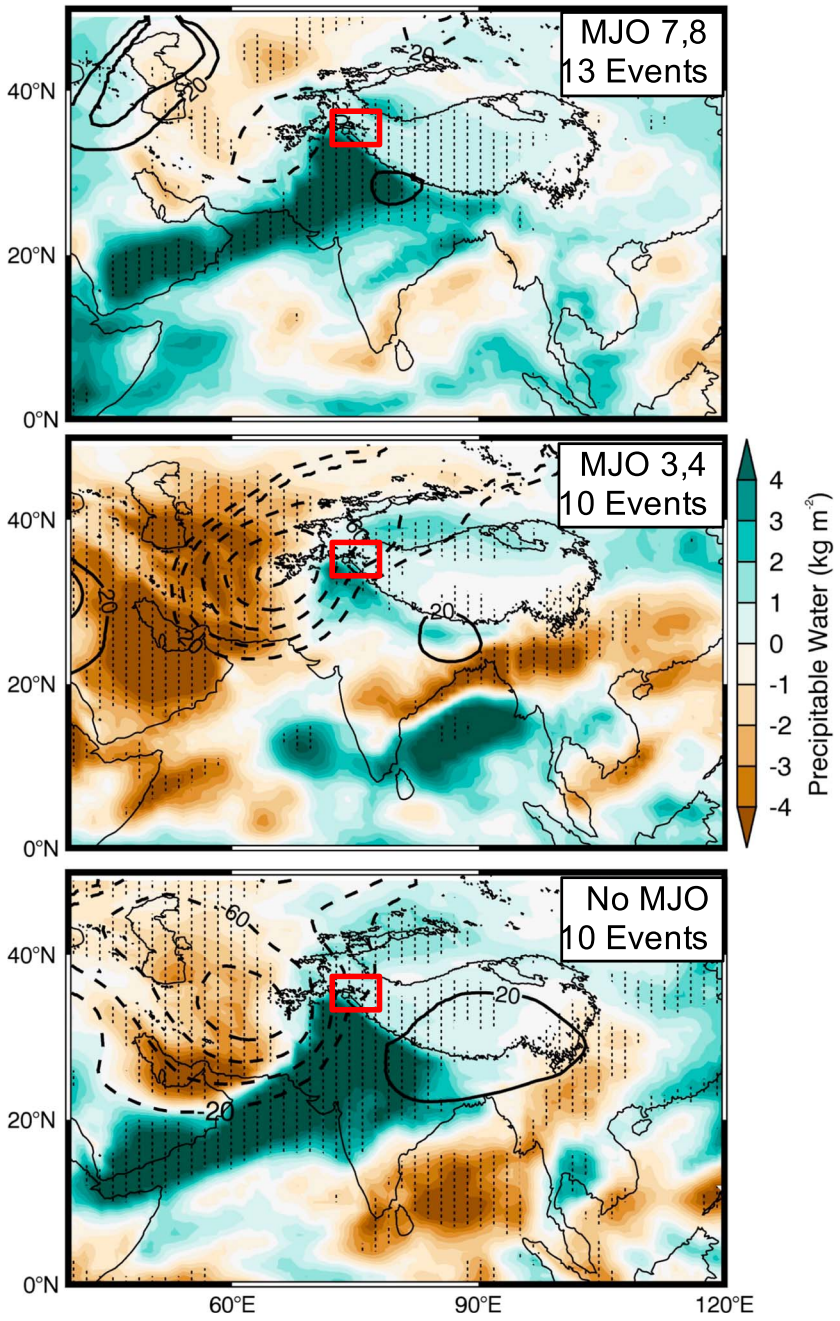

Figure 3. Composites of precipitable water anomalies (color) and 500 hPa geopotential height anomalies (contour; negative values are dashed) during extreme precipitation events in the Karakoram in MJO phases 7 and 8 with (top) ENSO neutral conditions, (middle) MJO phase 3/4 with ENSO neutral, and (bottom) neutral MJO and ENSO conditions. The red box identifies the precipitation-indexing region. Stippling indicates significance of precipitable water anomalies above the 95th percentile confidence interval.

that extends from equatorial Africa (significant anomalies in excess of 8 kg m^{-2} upstream of High Mountain Asia) compensates for reduced orographic forcing of precipitation. These composites illustrate the influence of tropical forcing on regional extreme events [*Cannon et al.*, 2016] but more importantly identify the influence of strong orographic forcing by well-developed cyclones and available moisture contributions to extreme precipitation, which are essential to examine individually in order to explain bias in coarse resolution topography simulation.

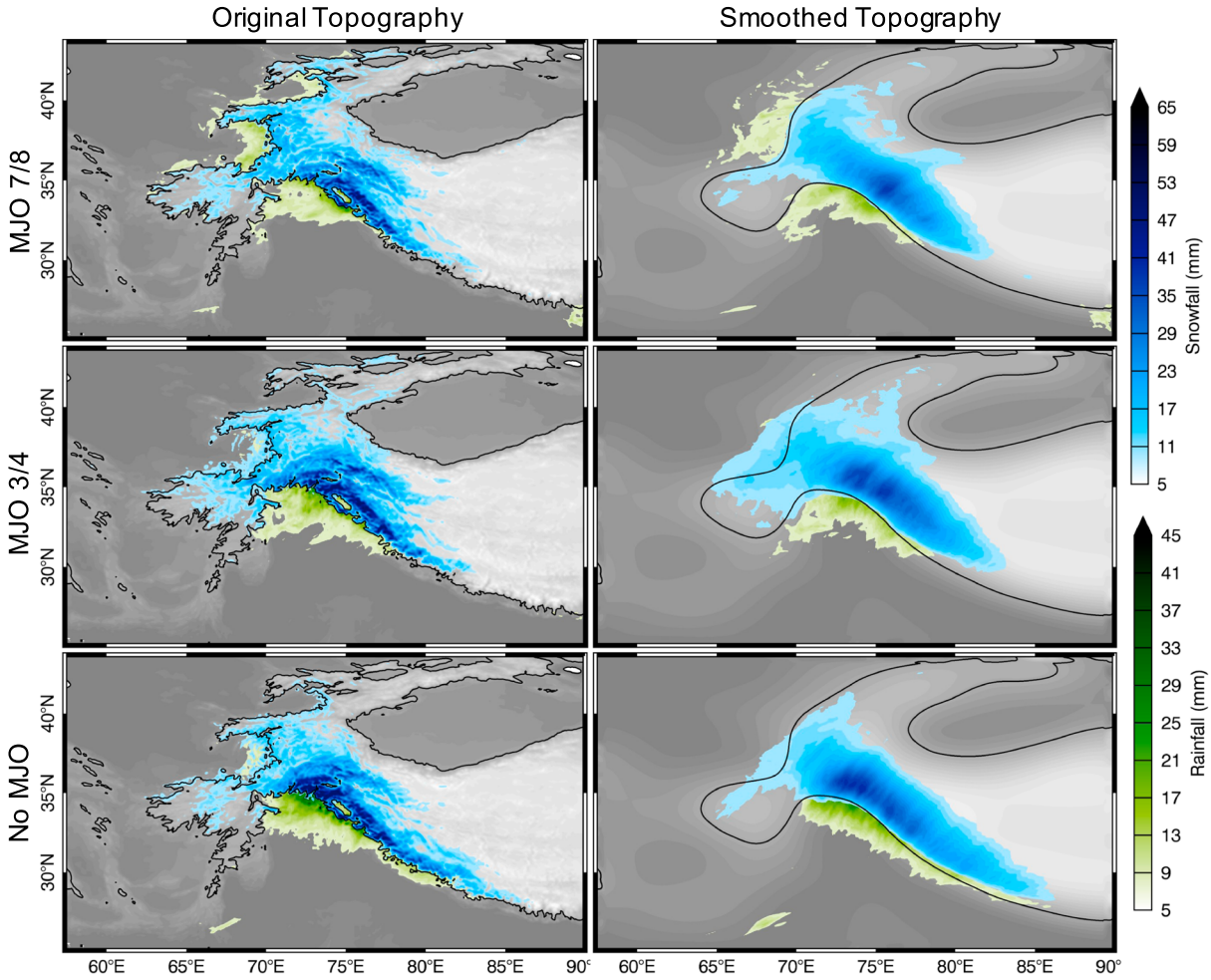

Figure 4. Composite rainfall (green) and snowfall (blue) during extreme precipitation events in the Karakoram in MJO phases 7 and 8 with (top row) ENSO neutral conditions, (middle row) MJO phase 3/4 with ENSO neutral, and (bottom row) neutral MJO and ENSO conditions. The 2000 m topography contour is outlined in black, and topography is shown as gray shade. (left column) Original topography experiments and (right column) modified topography experiments.

5. WRF Experiment Results and Discussion

5.1. Precipitation Distributions: Control Versus Modified Topography Experiments

Figure 4 demonstrates that the large-scale spatial distributions of both rainfall and snowfall are similar for all event categories and across experiment types, though coarse topography experiments exhibit considerable smoothing. Snowfall is plotted over rainfall, though we note that the transition margin between precipitation types is very thin due to steep topography. Despite similar spatial patterns, which are driven by the interaction of the WD with topography, it is notable that, locally, precipitation magnitudes are much greater in 6.67 km topography experiments for the western Himalaya and Karakoram ranges (the two bands of enhanced snowfall). *Mass et al.* [2002] identified similar orographic enhancement from 12 km to 4 km resolution simulations in the Cascades. Here the differences between simulations are also primarily attributable to topographic smoothing. However, Figure 4 identifies that precipitation covers a larger area in modified topography experiments, and quantitative analyses presented in the following sections demonstrate that total precipitation over High Mountain Asia increased in modified topography experiments.

5.2. Wind and Moisture Transects

5.2.1. Control Experiments

High-resolution WRF simulations of extreme events enable the investigation of thermodynamic and dynamic processes in the vertical and along individual slopes. Figure 5 shows composite cross sections of meridional wind for a transect across the western Himalaya and Karakoram at 73.5 E. Only one transect is

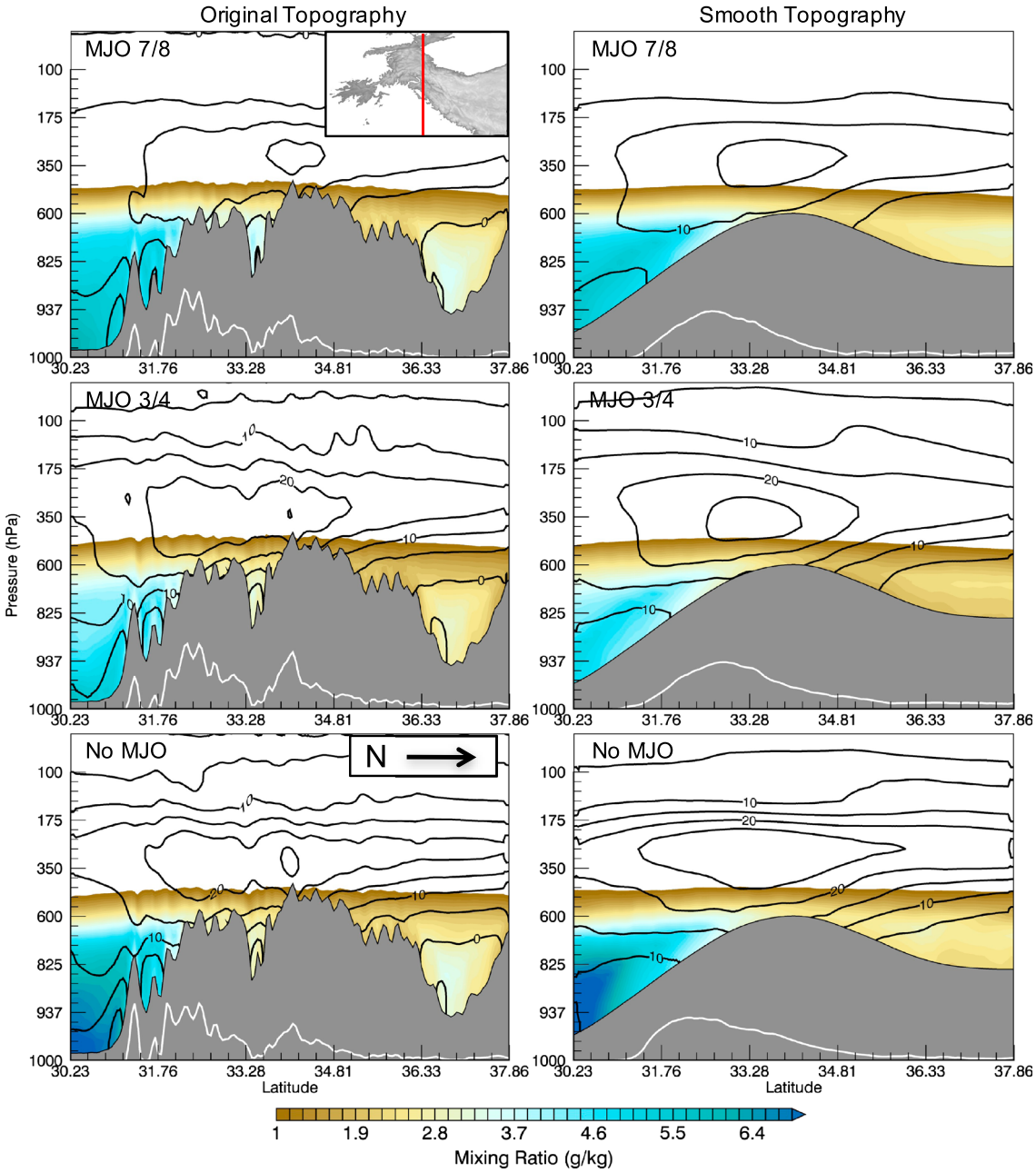

Figure 5. Vertical transect composites of mixing ratio (color) and meridional wind (contour) during extreme precipitation events in the Karakoram in MJO phases 7 and 8 with ENSO neutral conditions (top), MJO phase 3/4 with ENSO neutral (middle), and neutral MJO and ENSO conditions (bottom). Topography is shaded gray, and the white line indicates the location of snowfall accumulation (standardized by 80 mm maximum to show spatial distribution). (left column) Original topography experiments and (right column) modified topography experiments.

shown, though the differences observed between experiment types and event categories are consistent throughout the study region. The maximum value of southerly wind in the MJO 7/8 composite is 16 m s^{-1}, while in MJO 3/4 southerly wind exceeds 25 m s^{-1}, resulting in stronger topographically forced vertical motions (not shown).

Based on the precipitation distribution shown in Figures 4 and 5, it is clear that windward facing slopes receive the highest proportion of snowfall accumulation and that further downwind accumulation decreases at each subsequent orographic feature. The downwind decrease in precipitation can be explained by differences in the mixing ratio, which is considerably higher for extreme events in MJO phase 7/8. The snowfall

distributions are similar across event categories, despite considerable differences in dynamic and thermodynamic contributions to generating orographic precipitation, and are largely defined by first-order orographic effects [*Roe*, 2005]. In MJO phase 7/8 events, extreme precipitation is achieved despite relatively weak orographic forcing, largely on account of increased available moisture and reduced stability at the orographic barrier, as observed through theta-e profiles (discussed below in section 5.6). Extreme precipitation is generated in phase 3/4 events by comparatively strong vertical ascent on windward slopes (not shown), which effectively forces precipitation despite reduced moisture. Neutral-case events benefit from enhancements of both available moisture and cross-barrier wind speed, with mixing ratios exceeding 6.5 g kg^{-1} and southerly winds in excess of 25 m s^{-1} along the transect.

5.2.2. Modified Experiments

The general patterns of moisture availability and cross-barrier wind in modified topography experiments (Figure 5, right column) are similar across event types. However, differences in the strength of cross-barrier winds, the amount of available moisture, and the distribution of snowfall between original and modified topography experiments are evident. In all modified topography simulations, southerly wind is intensified and moisture propagates further north than in original topography simulations. The observed increase in the downstream mixing ratio is attributable to decreased precipitation efficiency and reduced water vapor depletion over smoothed topography [*Rutz et al*., 2015]. The area of 25 m s^{-1} (20 m s^{-1}) southerly wind aloft increases in size in the neutral and MJO 3/4 (7/8) composites. The elevation profile in the coarse topography experiments exhibits a single large hill, with precipitation peaking upstream of the crest and gradually tapering-off northward. The snowfall distribution of the 6.67 km topography experiment exhibits multiple maxima, colocated with windward ridges, while valleys receive relatively little precipitation due to gravity wave induced descent and evaporation [*Colle*, 2008]. The secondary maximum in precipitation in the original topography experiments, at the latitude of the Karakoram, benefits from moisture transported through the Indus river valley (Figure 4, left column). In the smooth topography case, precipitation at the approximate latitude of the Karakoram is in the lee of the single maximum that appears at approximately 3500 m elevation (Figure 4, right column).

5.3. Geopotential Height: Control Versus Modified Topography Experiments

The changes in cross-barrier wind speeds across experiment types shown in Figure 5 are explained by differences in the simulated development of WD. The influence of topographic smoothing on 500 hPa geopotential height anomalies associated with WD for each event category is shown in Figure 6. In smoothed topography simulations WD are dynamically stronger, as evidenced by deeper geopotential height anomalies. MJO 3/4 experiments with smoothed topography exhibited a deepening of the composite WD trough by more than 30 gpm. The center of each WD in all event categories recorded a lower 500 hPa geopotential height in the modified topography simulation than its original topography counterpart. The mean of the differences between trough depths in original and modified topography experiments, which were uniformly negative, were found to be significantly different from a hypothetical unbiased set of events (mean difference of zero) based on a *t* test ($p < 0.05$).

It is also important to note that the ridge ahead of the trough was significantly amplified in the modified topography simulations. The deeper troughs and more pronounced ridges of the modified topography experiments are evident in the enhanced dipole structure shown in Figure 6 (right column), which implies enhanced development of WD, an intensified geopotential height gradient, and intensified southerly cross-barrier winds over western High Mountain Asia (as observed in Figure 5). Topographic smoothing has a significant effect on WD dynamics here and has previously been shown to degrade the skill of mesoscale models in simulating extratropical cyclones near topography [*Wenygand and Seaman*, 1994]. The observed bias is possibly attributable to reduced mountain drag [*Carlson*, 1998], the effect of differences in mountain height on vorticity generation [*Holton and Hakim*, 2013], changes in baroclinicity related to reduced blocking of temperature advection, or a combination of factors, though these are not tested. Here we establish that the modification of the intensity of cross-barrier winds during the event is an important factor in determining the spatial and temporal distribution of precipitation.

5.4. Differences in Modified Topography Simulation

Prior work identified that moisture availability and cross-barrier winds are the primary determinants of the magnitude of orographic precipitation during WD [*Cannon et al*., 2015]. Figure 7 shows the spatial

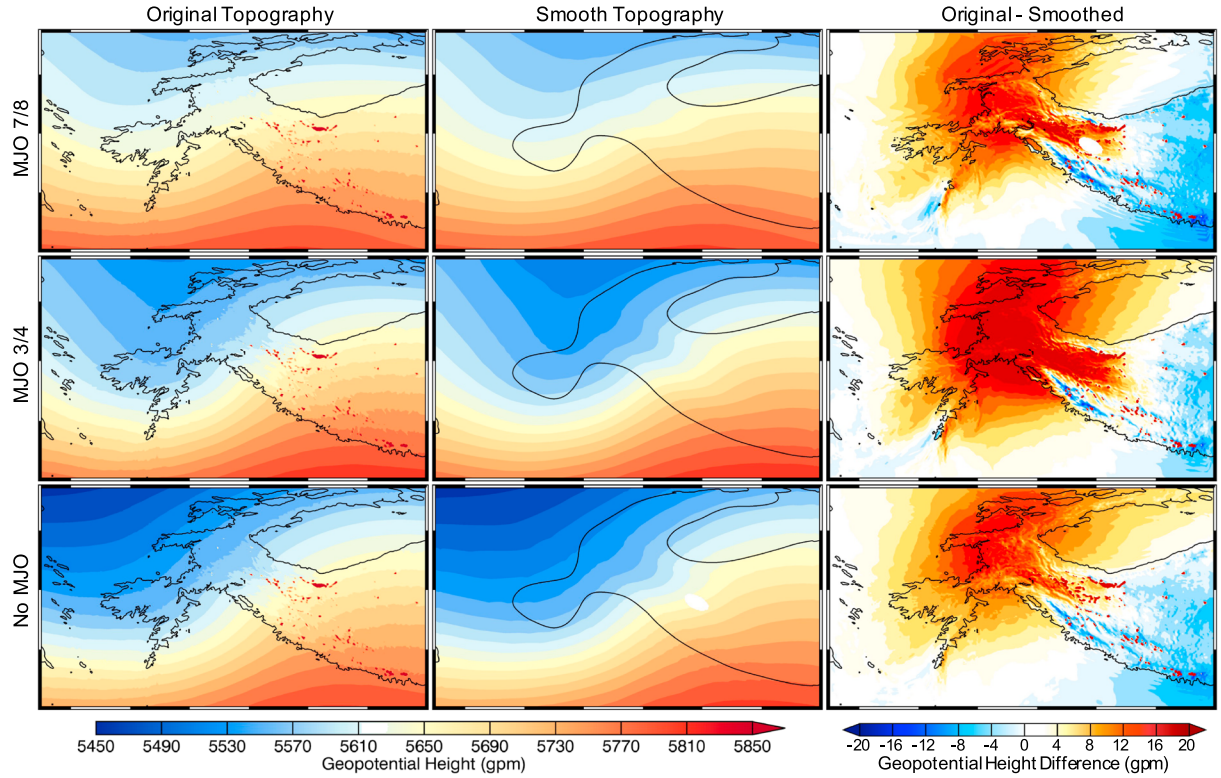

Figure 6. Composites of 500 hPa geopotential height during extreme precipitation events in the Karakoram in MJO phases 7 and 8 with ENSO neutral conditions (top), MJO phase 3/4 with ENSO neutral (middle), and neutral MJO and ENSO conditions (bottom). The 2000 m topography contour is outlined in black. (left column) Original topography experiments and (right column) modified topography experiments. The difference between the two experiment types is shown in Figure 6 (right column) for each event category.

distribution and magnitude of differences between modified topography simulations and control experiments for 2 m specific humidity, 500 hPa meridional winds, and snowfall for all 33 events, irrespective of category. The mean of the differences between original and modified topography experiments is shown only for significant grid points (*t* test; 5% significance level).

Topographic smoothing in modified topography experiments resulted in increased 2 m specific humidity over much of High Mountain Asia, primarily due to higher temperatures and saturation vapor pressure at lower altitudes. The entire Himalayan front exhibits a 2–3 g kg^{-1} increase in 2 m specific humidity in modified topography simulations, primarily because topography is lower and air temperature is higher; thus, the air holds more moisture (Clausius-Clapeyron relationship). Similarly, low-elevation areas adjacent High Mountain Asia and valleys in the interior of topography exhibit a decrease in humidity associated with increased surface elevation resulting from the smoothing/redistribution of High Mountain Asia's mountains. In addition to direct elevation changes, topographic smoothing results in less efficient blocking of moist flow and reduced water vapor depletion by orographic precipitation, allowing moisture to advect further into the interior. However, the smoothing of valley systems, such as the Indus River Valley, reduces moisture transport to the interior through these conduits [*Curio et al.*, 2014]. Moisture transport is discussed in detail in section 5.6.

Section 5.3 identified that topographic smoothing also alters WD strength. The intensified 500 hPa geopotential height gradient (Figure 6) in modified topography experiments is shown to enhance cross-barrier winds (Figure 7). The average magnitude of 500 hPa winds over the entire domain increased 7% in modified topography experiments (Table 1; discussed in detail section 5.5). Although topographic smoothing enhances WD dynamics and moisture availability, Figure 7 indicates that the maximum precipitation magnitudes are not enhanced in modified-topography simulation. Rather, precipitation is redistributed according to changes in topography and thus, orographic forcing. Generally, the steep slopes of the western Himalaya and Karakoram exhibit significant reductions in snowfall, while lower elevations experience

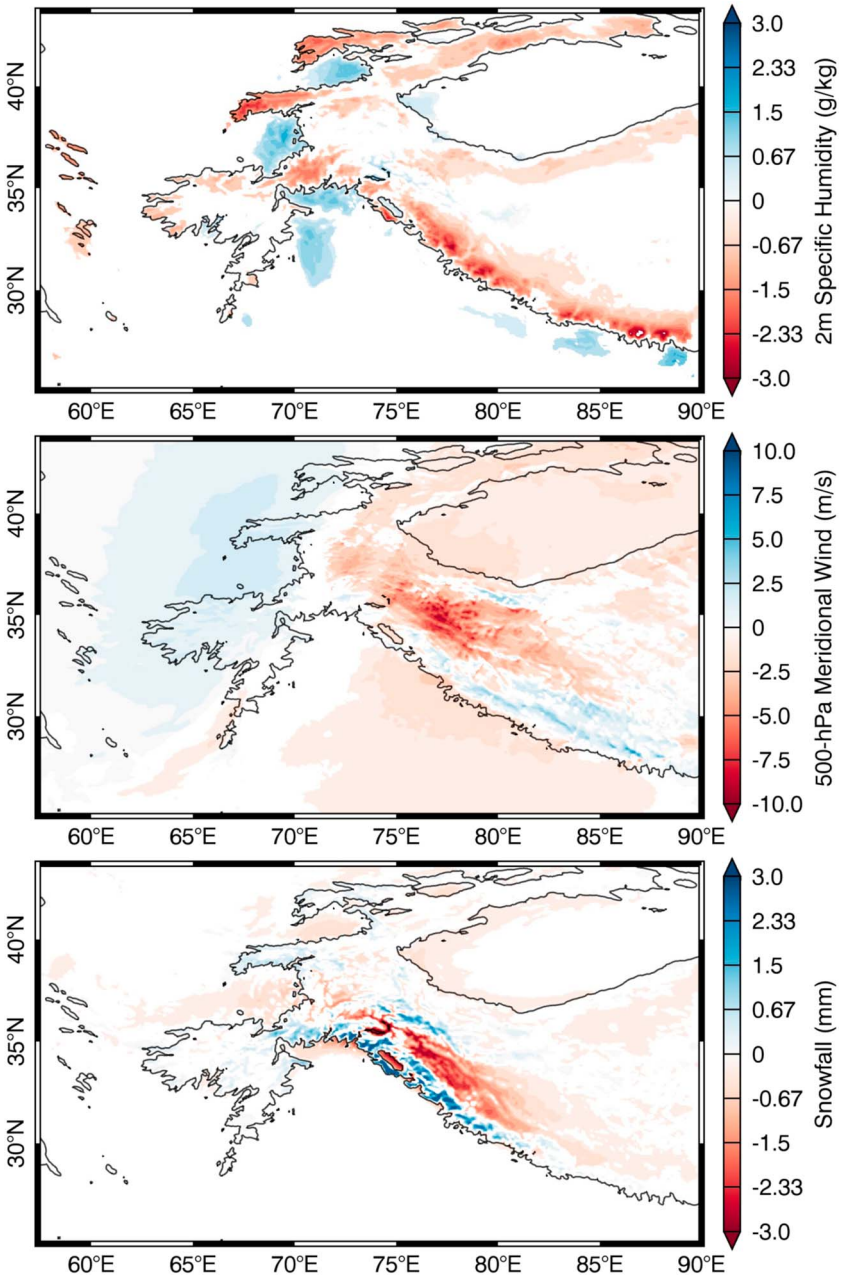

Figure 7. Statistically significant differences in 2 m specific humidity (top), 500 hPa meridional wind (middle), and snowfall (bottom) between original topography and modified topography simulations (all 33 events are included). Red values indicate a positive bias in modified topography experiments relative to original topography experiments.

significant increases, according to the redistribution of slopes that force orographic motions in the modified topography experiments (Figure 5). While the redistribution is not surprising, and could have been inferred by simply looking at the difference between topography, the following section demonstrates that changes in orographic forcing, WD dynamics, available moisture, and stability have significant influences over total accumulated precipitation in High Mountain Asia.

5.5. Effects of Simulation Differences on Orographic Forcing and Precipitation

Scatterplots of each event's averages of 2 m specific humidity, 500 hPa meridional wind, snowfall, and vertical wind speed, measured over the Karakoram region (limited to grid cells with fractional glacier cover (Figure 1) (Randolph Glacier Inventory V5.0 [*Arendt et al.*, 2015]) for original and modified topography simulations, are

Table 1. Statistics of Mean 2 m Specific Humidity, 500 hPa Meridional Wind, 500 hPa Vertical Wind, and Snowfall for the Greater Karakoram Study Region (Left) and the Glaciated, High-Elevation Regions of the Karakoram (Right)

	Karakoram				WRF Inner Domain			
	3/4	7/8	NEUT	ALL	3/4	7/8	NEUT	ALL
				Specific Humidity (g/kg)				
Original	2.04	2.29	1.98	2.12	3.12	3.93	3.6	3.59
Coarse	2.28	2.61	2.24	2.4	3.1	3.98	3.6	3.6
Difference	0.24	0.32	0.26	0.28[a]	−0.02	0.05	0	0.01
% Difference	12%	14%	13%	13%[a]	−1%	1%	0%	0%
				Meridional Wind (m/s)				
Original	18.25	10.31	18.45	15.18	8.23	5.64	7.56	7
Coarse	25.15	13.62	24.05	20.28	8.87	6.06	7.9	7.47
Difference	6.9[a]	3.31	5.6[a]	5.1[a]	0.64	0.42	0.34	0.47
% Difference	38%[a]	32%	30%[a]	34%[a]	8%	7%	4%	7%
				Vertical Velocity (m/s)				
Original	0.72	0.47	0.72	0.62	0.12	0.09	0.11	0.1
Coarse	0.07	0.06	0.07	0.06	0.037	0.03	0.036	0.034
Difference	−0.65[a]	−0.41[a]	−0.65[a]	−0.56[a]	−0.03[a]	−0.06[a]	−0.07[a]	−0.06[a]
% Difference	−90%[a]	−87%[a]	−90%[a]	−89%[a]	−69%[a]	−67%[a]	−67%[a]	−66%[a]
				Snowfall (mm)				
Original	34.87	32.73	25.6	31.22	2.51	2.08	2.31	2.28
Coarse	25.75	21.43	20.71	22.52	2.77	2.2	2.58	2.49
Difference	−9.12[a]	−11.3[a]	−4.89	−8.7[a]	0.26	0.12	0.27	0.21
% Difference	−26%[a]	−35%[a]	−19%	−28%[a]	10%	6%	12%	9%

[a]Significance based on a *t* test comparing the means of the two samples.

shown in Figure 8. Additionally, their statistics are displayed in Table 1. For glaciated areas of the Karakoram, located in the interior of topography and at high elevation, specific humidity differences between phases of the MJO are not as apparent as when the large scale is considered (Figure 3) because of more efficient drying of the moist flow over the first orographic barriers of the Himalaya via precipitation and considerable blocking of low-level flow. Grid points corresponding to the Karakoram have higher surface humidity amounts in smooth topography simulations than in the original simulations across all event categories, despite the fact that the Indus River Valley has been smoothed and does not serve as a moisture conduit. The average 2 m specific humidity increase in this region is approximately 13% (Table 1). Additionally, average 500 hPa southerly wind speeds for the same group of grid points are approximately 34% stronger in modified topography simulations, as noted earlier in this section based on composites. MJO 3/4 events, which had an average wind speed of 18.25 m s^{-1}, increased by 38%, while MJO 7/8 events, with an average wind speed of 10.31 m s^{-1}, increased 32%.

Despite positive differences in both moisture availability and orographic forcing in smooth topography experiments, vertical motions over the Karakoram in modified topography simulations are a fraction of the intensity exhibited in the original simulations. The average percentage decrease in the magnitude of vertical velocity was nearly 90% across all event categories. Given diminished vertical forcing, precipitation uniformly decreases in the modified topography simulations (average decrease of 28% across all event categories). Furthermore, because events in MJO phase 7/8 were already associated with relatively weak dynamical forcing, the reduction in orographic ascent velocities exacerbates the difference in accumulated snowfall in comparison to MJO phase 3/4 events, which see a slightly smaller reduction in snowfall on account of generally increased available moisture over lower and smoother topography (35% reduction in MJO 7/8 compared to 26% in MJO 3/4 and 19% in neutral cases).

In contrast to the high topography of the glaciated Karakoram, specific humidity over the entire domain exhibits a negligible difference between experiment types (Figure 8 and Table 1) because elevation, which is the primary moisture control, has been redistributed so that the mean is roughly the same. The spatial redistribution of moisture is discussed in detail in the following section. Additionally, the intensification of WD in modified topography experiments results in a uniform increase in the mean magnitude of 500 hPa winds in the domain, with an average increase of 7% (Table 1), though the mean magnitude of vertical

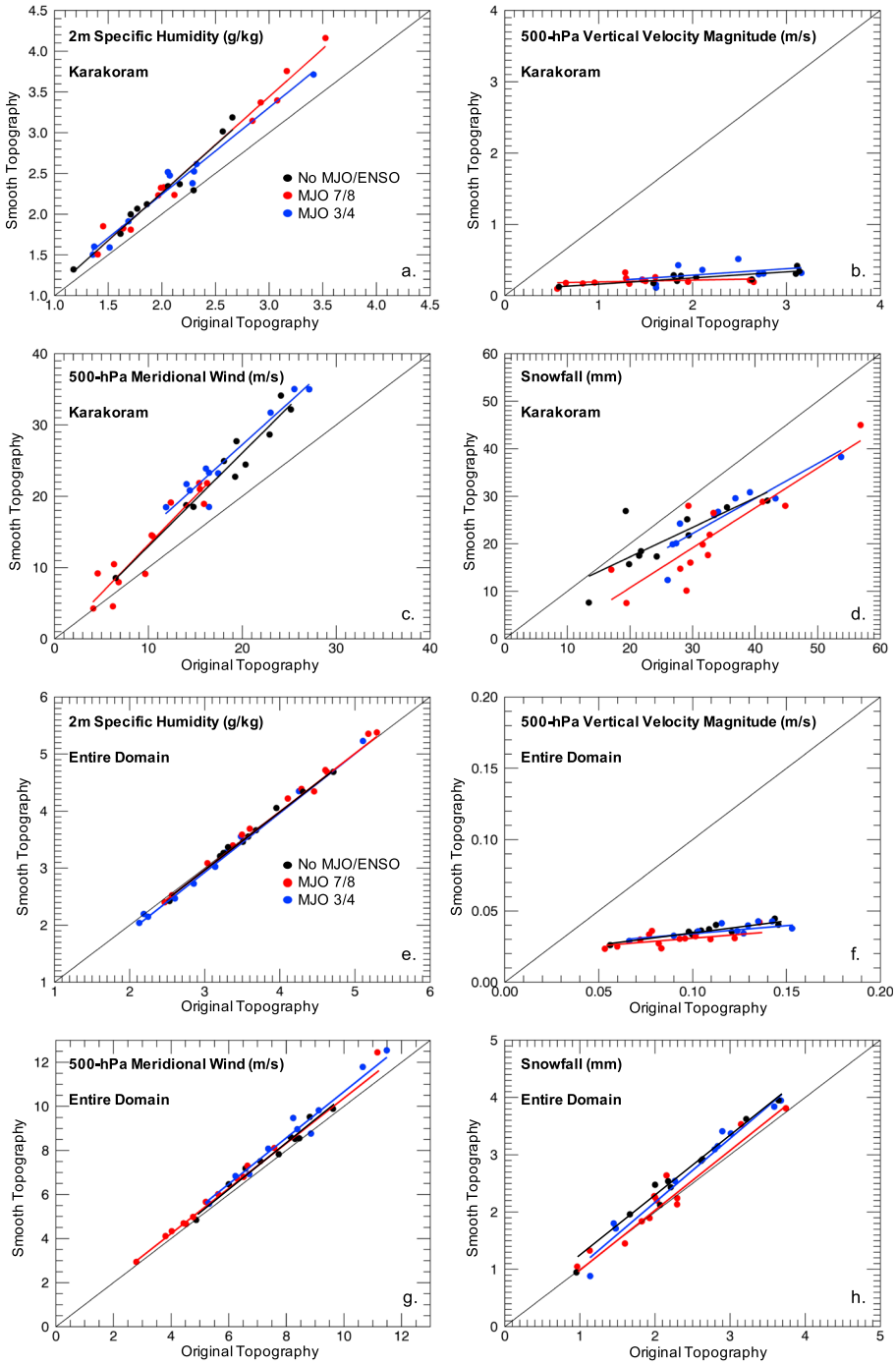

Figure 8. Scatterplots indicate original topography (*x* axis) and smoothed topography (*y* axis) simulated values of area-averaged 2 m specific humidity (a, e), 500 hPa meridional wind (c, g), 500 hPa vertical velocity magnitudes (absolute value; b, f), and snowfall (d, h) within the Karakoram (Figures 8a–8d) and the entire domain (Figures 8e–8h) for extreme precipitation events. Events are color coded according to MJO activity (Figure 8a), and a best fit line is drawn for each category.

velocity was reduced by 67%. Despite reduced vertical velocities on account of topographic smoothing, snowfall increased by an average of 9% across the entire domain (rainfall increases by 6%; not shown). This result is explained through differences in vapor transport and stability in the two experiment types in the following section.

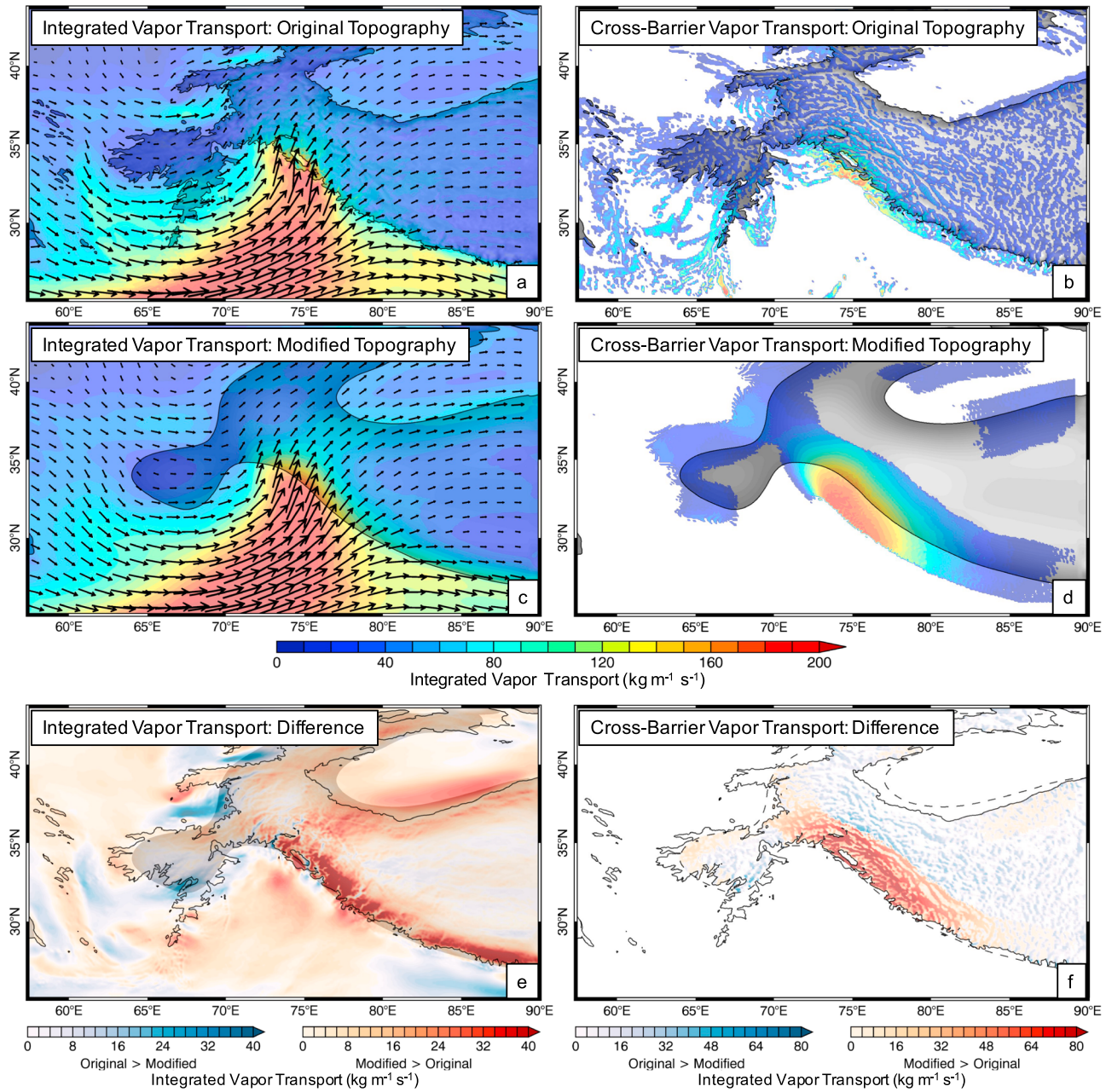

Figure 9. (a, c) Average vertically integrated moisture flux magnitude and direction for 33 extreme events across all event categories. (b, d) Average cross-barrier component of moisture flux. Original topography experiment results appear in Figures 9a and 9b and modified topography results in Figures 9c and 9d. Figures 9e and 9f show (e) the difference in moisture flux magnitude between original and modified topography experiments and (f) the difference in the cross-barrier component of moisture flux above 2000 m between experiment types. The 2000 m elevation contour is shaded and outlined for each figures respective topography.

5.6. Vapor Transport and Stability

The average integrated vapor transport of all 33 extreme events is shown in Figure 9 for the original and modified topography experiments. The difference between these composites illustrates that reduced blocking in the modified topography experiments allows for the transport of moisture further into topography, with the largest differences observed at and downstream of the Himalaya. Figures 9b, 9d, and 9f show cross-barrier vapor transport, which was calculated by projecting vapor transport into the cross-barrier direction for slopes greater than 2% and with an aspect less than 90° different than the direction of vapor transport. This highlights the magnitude of vapor transport that undergoes orographic lifting. The difference between original

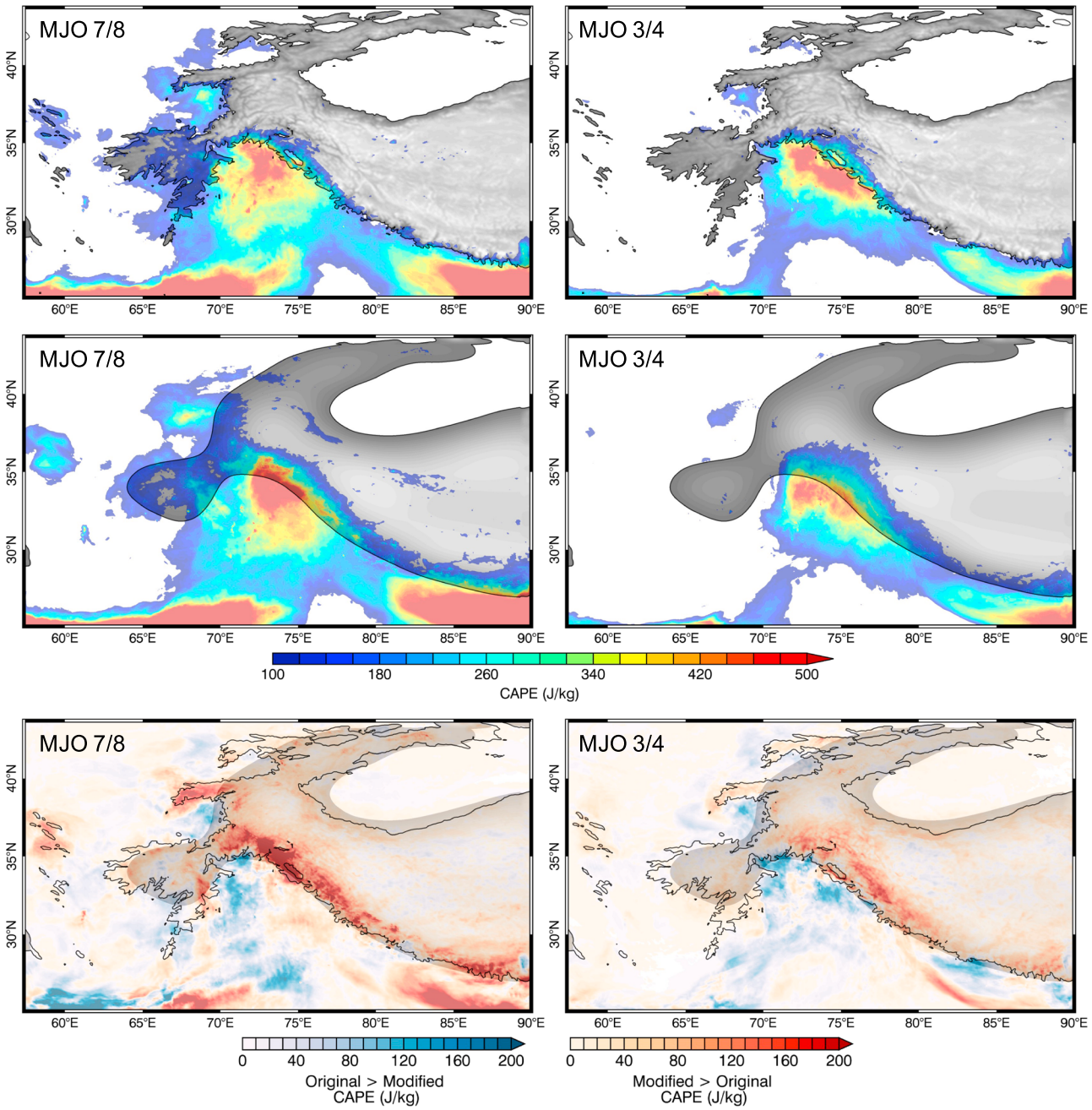

Figure 10. CAPE values for extreme events in MJO phases 7/8 (left column) and 3/4 (right column) under original (top row) and modified (middle row) topography conditions. Differences between experiment types are shown in the bottom row. The 2000 m elevation contour for experiment types is shaded and outlined.

and modified topography experiments shows that the amount of vapor transport impinging on topography and being forced to rise is considerably larger in the modified topography simulations. While orographic forcing over smooth topography is considerably reduced, and precipitation rates are smaller, the total vapor transport over the entire domain is enhanced by 8% in smooth topography simulations, largely due to intensified WD dynamics. The cross-barrier vapor transport is increased by 19%, and the cross-barrier vapor transport above 2000 m elevation is increased by 14% on account of both stronger wind speed and reduced depletion of water vapor by orographic precipitation [*Rutz et al.*, 2015].

Increased near-surface heat and moisture content at high elevations in the modified topography experiments also impacts atmospheric stability. Figure 10 shows convectively available potential energy (CAPE)

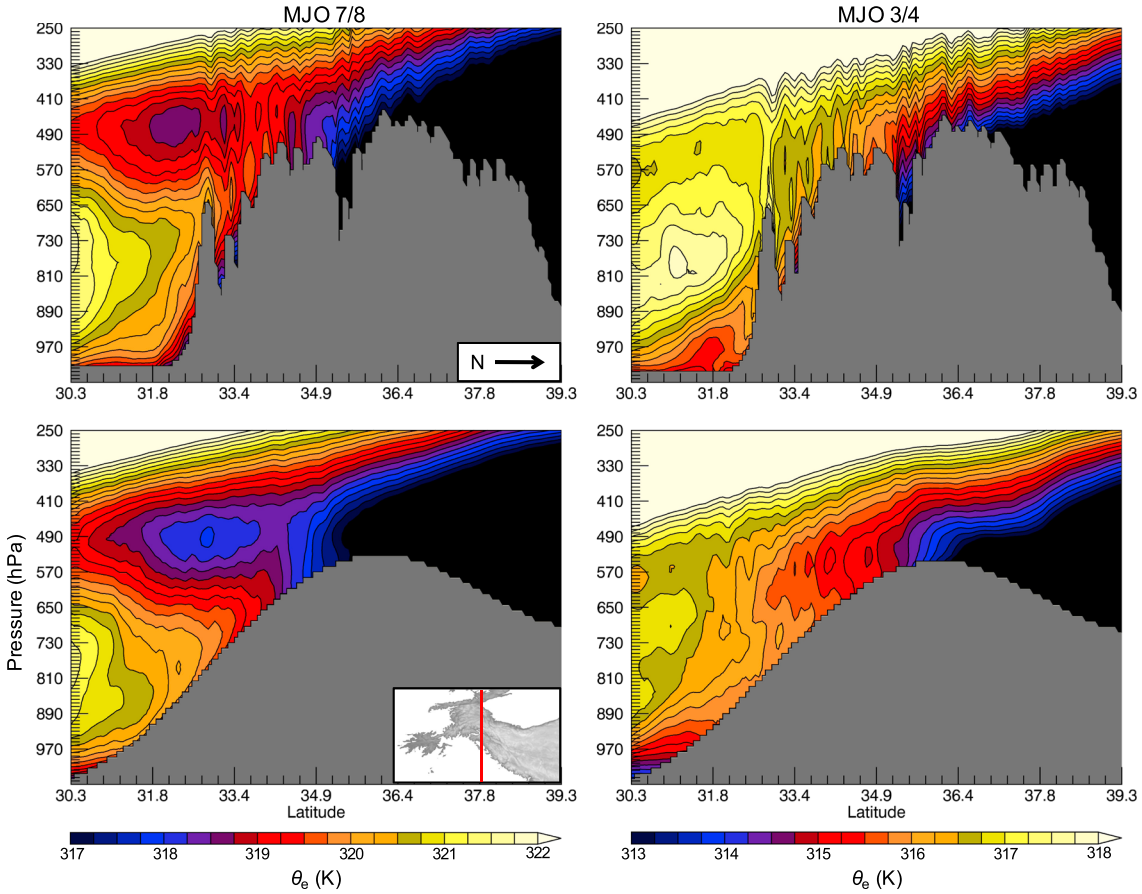

Figure 11. Vertical transect of equivalent potential temperature (θ_e) for events in MJO phases 7/8 (left column) and 3/4 (right column) under original (top row) and modified (middle row) topography conditions. Topography is shaded gray.

composites of extreme events in MJO phases 7/8 and 3/4, for both original and modified topography simulations. While CAPE values in the composites are generally low, values for foothill regions of High Mountain Asia were observed in excess of 2000 J/kg at 1 h temporal resolution during individual MJO 7/8 events (not shown). CAPE is included to illustrate spatial differences of atmospheric stability as a vertical integral. The difference between experiment types indicates that the enhanced transport of warm and moist air to high elevations in the smooth topography simulations (Figure 9) creates conditions over the southern portion of High Mountain Asia that are comparatively less stable. Vertical transects of equivalent potential temperature across the western Himalaya and Karakoram (Figure 11) identify increased near-surface values in smooth topography experiments relative to original topography simulations in both MJO 7/8 and 3/4 composites. The color scale is stretched to emphasize gradients over the southern slope of High Mountain Asia. In the MJO 3/4 smooth topography composites the advection of warm moist air upslope is seen to reduce the vertical gradient of θ_e between 900 and 500 hPa above the south facing slope. Additionally, the deepening of the upper level trough in smooth topography simulations (section 5.3) decreases temperature aloft in both MJO 7/8 and 3/4 composites, thus further reducing the vertical gradient of equivalent potential temperature and enhancing instability. The difference in CAPE between experiment types is most dramatic for the MJO 7/8 events (Figure 10), which contain comparatively more heat and moisture than MJO 3/4 events.

In these simulations, the effect of reduced orographic forcing on precipitation that results from smooth topography is partially mitigated by the bias toward enhanced thermodynamic mechanisms. This is especially evident in MJO phases 7 and 8. Based on the 9% increase in precipitation over the entire study domain in modified topography simulation (Table 1), it appears that the effect of increased cross-barrier moisture flux and instability over smooth topography exceeds that of reduced orographic uplift on precipitation totals. While precipitation rates in smooth topography simulations do not rival those of original topography

simulations over the western Himalaya and Karakoram's steep slopes, the aggregated effect of enhanced vapor transport on precipitation over High Mountain Asia results in a positive bias, and more importantly, illustrates differences in precipitation mechanisms according to topographic resolution.

6. Caveats

The results of this study are not directly comparable with many idealized experiment studies, which typically evaluate the influence of changes in dynamical forcing or moisture availability independently from changes in topography, in order to isolate their effects across experiment types [e.g., *Colle*, 2008]. The present study is unique in that the mechanisms that drive precipitation are significantly biased in modified topography experiments. Furthermore, total precipitation over High Mountain Asia is sensitive to a large number of mesoscale phenomena and microphysical processes [e.g., *Medina and Houze*, 2003]. It is beyond the scope of this paper to isolate the individual influences of each of these. While computational costs limited the number of experiments that could be performed, it is clear that topographic smoothing significantly alters the simulation of WD dynamics and biases the representation of physical mechanisms that drive orographic precipitation in High Mountain Asia, based on changes in large-scale circulation, mesoscale orographic forcing, and thermodynamic influences.

7. Conclusions

This manuscript investigates the importance of topographic resolution in simulating the physical mechanisms that generate extreme winter precipitation events in High Mountain Asia using the Weather Research and Forecasting model (WRF). A set of experiments was performed comparing WRF simulation of extreme precipitation events with varying model topography. Simulations of 33 extreme events were performed for two experiment groups using (1) native model-resolution topography (6.67 km) and (2) smoothed topography from a global circulation model (GCM; $1.875° \times 1.25°$). WRF was configured to control for the effects of horizontal resolution by maintaining 6.67 km resolution for both original and modified topography experiments. The 33 simulated westerly disturbance (WD) events were selected from 205 independent 90th percentile extreme events in the period 1979–2012 based on three unique categories of dynamical and thermodynamic contributions to precipitation.

Our investigation resulted in the following key findings on the influence of topographic smoothing on meteorological simulation:

1. Smooth topography allows for the intensification of atmospheric circulation associated with WD and generates stronger cross-barrier winds.
2. Intensified cross-barrier winds in WD and reduced topographic blocking enable enhanced vapor transport to high elevations of High Mountain Asia. This, in turn, increases available moisture and reduces stability during extreme precipitation events.
3. Smooth topography generates only a fraction of the orographic ascent observed in original topography simulations of WD, thus reducing maximum precipitation rates and total precipitation over steep topography. An approximately 28% reduction in precipitation was observed across all event categories in the Karakoram.
4. Total precipitation over the study domain is 9% greater in smoothed topography experiments, indicating that the effects of enhanced moisture transport and thermodynamics over a broad and moderate slope outweigh the negative effect of reduced orographic lift on precipitation, where steep windward slopes were smoothed.

While the magnitude of the statistics presented may be sensitive to the chosen smoothing technique and resolution in the modified topography experiments, the dynamical and thermodynamic processes that underlie the relationship between topographic smoothing and High Mountain Asia meteorology during WD events are likely robust. This research emphasizes a physical basis to investigate the effect of topographic smoothing on the simulation of precipitation rather than focusing on statistical differences alone. In summary, simulations with smoothed topography exhibit significant biases in their representations of WD dynamics, enhanced large-scale thermodynamic precipitation mechanisms, and unrealistic precipitation in High Mountain Asia.

These findings challenge the ability of coarse resolution GCMs to resolve orographic precipitation processes in High Mountain Asia, and the observed intensification of WD dynamics, moisture transport to high elevations, and instability in smooth topography experiments pose a possible explanation for their positive regional precipitation bias [*Palazzi et al*., 2014]. It is also likely that the effect of topographic smoothing on cyclone dynamics manifests downstream of the mountains, thus influencing the simulation of global storm tracks. It appears that the suite of GCMs that have been used to produce ensemble-mean climate projections for water resource applications in High Mountain Asia (reviewed in *Miller et al*. [2012]) do not realistically simulate extreme winter precipitation events. These results also show that biases in precipitation simulation are unique according to the prevailing atmospheric conditions. The influences of tropical forcing and seasonality on WD dynamics and moisture availability are thus a considerable source of uncertainty in defining GCM bias. Furthermore, future changes in moisture availability [*Held and Soden*, 2006] or storm tracks [*Hartmann et al*., 2013] affecting High Mountain Asia may produce unrealistic changes in precipitation based on the poor representation of the relationships between moisture availability, dynamical forcing, and orographic precipitation in smooth topography experiments. The identification of model bias is essential to effectively utilizing GCMs to study the future fate of water resources in High Mountain Asia and beyond.

Acknowledgments

This research was supported by the Climate and Large-Scale Dynamics Program, from the National Science Foundation (NSF award AGS 1116105) and by NASA Headquarters under the NASA Earth and Space Science Fellowship Program (grant 13-EARTH13F-26). The CFSR data used in this research were developed by NOAA's National Centers for Environmental Prediction (NCEP) and provided by NCAR. All WRF model output generated for this study is available upon request through an FTP hosted by the Earth Research Institute at the University of California, Santa Barbara. Please email Forest Cannon (fcannon@eri.ucsb.edu) for data access. The authors also thank three anonymous reviewers for their helpful comments and suggestions for improving the manuscript.

References

Anders, A. M., G. H. Roe, B. Hallet, D. R. Montgomerey, N. J. Finnegan, and J. Putkonen (2006), Spatial patterns of precipitation and topography in the Himalaya, *Geol. Soc. Am. Spec. Pap.*, *398*, 39–53.

Arendt, A., et al. (2015), Randolph Glacier Inventory—A dataset of global glacier outlines: Version 5.0, Global Land Ice Measurements from Space, Digital Media, Boulder, Colo.

Barlow, M., M. Wheeler, B. Lyon, and H. Cullen (2005), Modulation of daily precipitation over southwest Asia by the Madden-Julian oscillation, *Mon. Weather Rev.*, *133*, 3579–3594.

Barros, A. P., S. Chiao, T. J. Lang, D. Burbank, and J. Putkonen (2006), From weather to climate—Seasonal and interannual variability of storms and implications for erosion processes in the Himalaya, *Geol. Soc. Am. Spec. Pap.*, *398*, 17–38.

Bookhagen, B., and D. W. Burbank (2010), Towards a complete Himalayan hydrological budget: The spatiotemporal distribution of snow melt and rainfall and their impact on river discharge, *J. Geophys. Res.*, *115*, F03019, doi:10.1029/2009JF001426.

Cannon, F., L. M. V. Carvalho, C. Jones, and B. Bookhagen (2014), Multi-annual variations in winter westerly disturbance activity affecting the Himalaya, *Clim. Dyn.*, *44*, 441–455.

Cannon, F., L. M. V. Carvalho, C. Jones, and J. Norris (2015), Winter westerly disturbance dynamics and precipitation in the western Himalaya and Karakoram: A wave-tracking approach, *Theor. Appl. Climatol.*, doi:10.1007/s00704-015-1489-8.

Cannon, F., L. M. V. Carvalho, C. Jones, A. Hoell, J. Norris, G. Kiladis, and A. A. Tahir (2016), The influence of tropical forcing on extreme winter precipitation in the western Himalaya, *Clim. Dyn.*, doi:10.1007/s00382-016-3137-0.

Carlson, T. N. (1998), *Mid-Latitude Weather Systems*, pp. 195, American Meteorological Society, Boston.

Colle, B. A. (2008), Two-dimensional idealized simulations of the impact of multiple windward ridges on orographic precipitation, *J. Atmos. Sci.*, *65*, 509–523.

Curio, J., F. Maussion, and D. Scherer (2014), A twelve-year high-resolution climatology of atmospheric water transport on the Tibetan Plateau, *Earth Syst. Dynam.*, *6*, 109–124.

Dimri, A. P., D. Niyogi, A. P. Barros, J. Ridley, U. C. Mohanty, T. Yasunari, and D. R. Sikka (2015), Western disturbances: A review, *Rev. Geophys.*, *53*, 225–246, doi:10.1002/2014RG000460.

Dudhia, J. (1989), Numerical study of convection observed during the Winter Monsoon Experiment using a mesoscale two-dimensional model, *J. Atmos. Sci.*, *46*, 3077–3107.

Farr, T. G., et al. (2007), The shuttle radar topography mission, *Rev. Geophys.*, *45*, RG2004, doi:10.1029/2005RG000183.

Gao, X., Y. Xu, Z. Zhao, J. S. Pal, and F. Giorgi (2006), On the role of resolution and topography in the simulation of East Asia precipitation, *Theor. Appl. Climatol.*, *86*, 173–185.

Giorgi, F., and M. R. Marinucci (1996), Investigation of the sensitivity of simulated precipitation to model resolution and its implications for climate studies, *Mon. Weather Rev.*, *124*, 148–166.

Gutmann, E. D., R. M. Rasmussen, C. Liu, K. Ikeda, D. Gochis, M. P. Clark, J. Dudhia, and G. Thompson (2012), A comparison of statistical and dynamical downscaling of winter precipitation over complex terrain, *J. Clim.*, *25*, 262–281.

Hartmann, D. L., et al. (2013), Observations: Atmosphere and surface, in *Climate Change 2013: The Physical Science Basis. Contribution of Working Group I to the Fifth Assessment Report of the Intergovernmental Panel on Climate Change*, edited by T. F. Stocker et al., Cambridge Univ. Press, Cambridge, New York.

Held, I. M., and B. J. Soden (2006), Robust responses of the hydrological cycle to global warming, *J. Clim.*, *19*, 5686–5699.

Hewitt, K. (2014), *Glaciers of the Karakoram Himalaya: Glacial Environments, Processes, Hazards and Resources*, Springer, Dordrecht, Netherlands.

Hoell, A., M. Barlow, M. C. Wheeler, C. Funk (2014), Disruption of El Nino-Southern Oscillation teleconnections by the Madden Julian Oscillation, *Geophys. Res. Lett.*, *41*, 998–1004, doi:10.1002/2013GL058648.

Holton, J. R., and G. J. Hakim (2013), An Introduction to Dynamic Meteorology, 5th ed., Academic Press, Amsterdam.

Hong, S. Y., Y. Noh, and J. Dudhia (2006), A new vertical diffusion package with an explicit treatment of entrainment processes, *Mon. Weather Rev.*, *134*, 2318–2341.

Jones, C. (2009), A homogeneous stochastic model of the Madden-Julian Oscillation, *J. Clim.*, *22*, 3270–3288.

Kain, J. S. (2004), The Kain-Fritsch convective parameterization: An update, *J. Appl. Meteorol.*, *43*, 170–181.

Kapnick, S. B., T. L. Delworth, M. Ashfaq, S. Malyshev, and P. C. D. Milly (2014), Snowfall less sensitive to warming in Karakoram than in Himalayas due to unique seasonal cycle, *Nat. Geosci.*, *7*, 834–840.

Lang, T. J., and A. P. Barros (2004), Winter storms in the central Himalayas, *J. Meteorol. Soc. Jpn.*, *82*, 829–844.

Lutz, A. F., W. W. Immerzeel, A. Gobiet, F. Pellicciotti, and M. F. P. Bjerkens (2013), Comparison of climate change signals in CMIP3 and CMIP5 multi-model ensembles and implications for central Asian glaciers, *Hydrol. Earth Syst. Sci.*, *17*, 3661–3677.
Madden, R., and P. Julian (1972), Description of global-scale circulation cells in the tropics with a 40–50 day period, *J. Atmos. Sci.*, *29*, 1109–1123.
Martin, G. M., et al. (2011), The HadGEM2 family of Met Office unified model climate configurations, *Geosci. Model. Dev.*, *4*, 723–757.
Mass, C., D. Ovens, M. Albright, and K. Westrick (2002), Does increasing horizontal resolution produce better forecasts? The results of two years of real-time numerical weather prediction in the Pacific Northwest, *Bull. Am. Meteorol. Soc.*, *83*, 407–430.
Maussion, F., D. Scherer, T. Molg, E. Collier, J. Curio, and R. Finkelnburg (2014), Precipitation seasonality and variability over the Tibetan Plateau as resolved by the High Mountain Asia reanalysis, *J. Clim.*, *27*, 1910–1927.
Medina, S., and R. Houze (2003), Air motions and precipitation growth in alpine storms, *Q. J. R. Meteorol. Soc.*, *129*, 345–371.
Miller, J. D., W. W. Immerzeel, and G. Rees (2012), Climate change impacts on glacier hydrology and river discharge in the Hindu Kush-Himalayas: A synthesis of the scientific basis, *Mt. Res. Dev.*, *32*, 461–467.
Mlawer, E. J., S. J. Taubman, P. D. Brown, M. J. Iacono, and S. A. Clough (1997), Radiative transfer for inhomogeneous atmospheres: RRTM, a validated correlated-k model for the longwave, *J. Geophys. Res.*, *102*, 16,663–16,682, doi:10.1029/97JD00237.
Monin, A. S., and A. M. Obukhov (1954), Basic laws of turbulent mixing in the surface layer of the atmosphere, *Tr. AKad Nauk SSSR Geofiz. Inst.*, *24*, 163–187.
Niu, G. Y., et al. (2011), The community Noah land surface model with multiparameterization options (Noah-MP): 1. Model description and evaluation with local-scale measurements, *J. Geophys. Res.*, *116*, D12109, doi:10.1029/2010JD015139.
Norris, J., L. M. V. Carvalho, C. Jones, and F. Cannon (2015), WRF simulations of two extreme snowfall events associated with contrasting extratropical cyclones over the Himalayas, *J Geophys Res. Atmos.*, *120*, 3114–3138, doi:10.1002/2014JD022592.
Norris, J., L. M. V. Carvalho, C. Jones, F. Cannon, and B. Bookhagen (2016), The spatiotemporal variability of precipitation in the Himalaya: Validation of a one-year WRF model simulation, *Clim. Dyn.*, doi:10.1007/s00382-016-3414-y.
Palazzi, E., J. von Hardenberg, and A. Provenzale (2013), Precipitation in the Hindu-Kush Karakoram Himalaya: Observations and future scenarios, *J. Geophys. Res. Atmos.*, *118*, 85–100, doi:10.1029/2012JD018697.
Palazzi, E., J. von Hardenberg, S. Terzago, and A. Provenzale (2014), Precipitation in the Karakoram-Himalaya: A CMIP5 view, *Clim. Dyn.*, *45*, 21–45.
Park, S., and R. Schowengerdt (1983), Image reconstruction by parametric cubic convolution, *Comput. Vis. Graph. Im. Proc.*, *23*, 258–272.
Ridley, J., A. Wiltshire, and C. Mathison (2013), More frequent occurrence of westerly disturbances in Karakoram up to 2100, *Sci. Total Environ.*, *468-469*, S31–S35.
Roe, G. H. (2005), Orographic precipitation, *Annu. Rev. Earth Planet. Sci.*, *33*, 647–671.
Rutz, J. J., W. J. Steenburgh, and F. M. Ralph (2015), The inland penetration of atmospheric rivers over western North America: A Lagrangian analysis, *Mon. Weather Rev.*, *143*, 1924–1944.
Saha, S., et al. (2010), The NCEP climate forecast system reanalysis, *Bull. Am. Meteorol. Soc.*, *91*, 1015–1057.
Shea, J. M., W. W. Immerzeel, P. Wagnon, C. Vincent, and S. Bajracharya (2015), Modelling glacier change in the Everest region, Nepal Himalaya, *Cryosphere*, *9*, 1105–1128.
Singh, P., K. S. Ramasastri, and N. Kumar (1995), Topographical influence on precipitation distribution in different ranges of western Himalayas, *Nord. Hydrol.*, *26*, 259–284.
Skamarock, W. C., B. J. Klemp, J. Dudhia, D. O. Gill, D. M. Barker, M. G. Duda, X. Y. Huang, W. Wang, and J. G. Powers (2008), A description of the advanced research WRF version 3, NCAR Technical Note – 4751STR
Soncini, A., et al. (2015), Hydrology of the upper Indus Basin under potential climate change scenarios, *Engineering Geology for Society and Territory*, pp. 43–49, Springer, Switzerland.
Su, F., L. Zhang, T. Ou, D. Chen, T. Yao, K. Tong, and Y. Qi (2016), Hydrological response to future climate changes for the major upstream river basins in the Tibetan Plateau, *Global Planet. Change*, *136*, 82–95.
Tahir, A. A., P. Chevallier, Y. Arnaud, and B. Ahmad (2011), Snow cover dynamics and hydrological regime of the Hunza River basin, Karakoram Range, northern Pakistan, *Hydrol. Earth Syst. Sci.*, *15*, 2275–2290.
Thompson, G., P. R. Field, R. M. Rasmussen, and W. D. Hall (2008), Explicit forecasts of winter precipitation using an improved bulk microphysics scheme. Part II: Implementation of a new snow parameterization, *Mon. Weather Rev.*, *136*, 5095–5115.
Wehner, M. (2013), *Methods of Projecting Future Changes in Extremes*, Extremes in a Changing Climate, 223–237, Springer, Netherlands.
Wenygand, S. S., and N. L. Seaman (1994), Quantification of predictive skill for mesoscale and synoptic scale meteorological features as a function of horizontal grid resolution, *Mon. Weather Rev.*, *122*, 57–71.
Wilks, D. S. (2006), *Statistical Methods in the Atmospheric Sciences*, Elsevier, Burlington.
World Climate Research Program Coupled Model Intercomparison Project – Phase 5 (CMIP5), (2011), CLIVAR exchanges 56, vol. 16, 32 pp.
Wulf, H., B. Bookhagen, and D. Scherler (2016), Differentiating between rain, snow, and glacier contributions to river discharge in the western Himalaya using remote-sensing data and distributed hydrological modeling, *Adv. Water Resour.*, *88*, 152–169.
Yorgun, M. S., and R. B. Rood (2015), An object-based approach for quantification of GCM biases of the simulation of orographic precipitation. Part I: Idealized simulations, *J. Clim.*, *27*, 9139–9154.